Available online at www.sciencedirect.com
SCIENCE DIRECT®
Journal of Solid State Chemistry 178 (2005) 1–7
JOURNAL OF SOLID STATE CHEMISTRY
www.elsevier.com/locate/jssc

XRD and ^{29}Si MAS-NMR spectroscopy across the β-$Lu_2Si_2O_7$–β-$Y_2Si_2O_7$ solid solution

Ana I. Becerro*, Alberto Escudero

Departamento de Química Inorgánica-Instituto de Ciencia de Materiales de Sevilla, Universidad de Sevilla-CSIC. Avda. Américo Vespucio, s/n. 41092 Sevilla, Spain

Received 19 July 2004; received in revised form 9 September 2004; accepted 10 September 2004

Abstract

Samples in the system $Lu_{2-x}Y_xSi_2O_7$ ($0 \leqslant x \leqslant 2$) have been synthesized following the sol–gel method and calcined to 1300 °C, a temperature at which the β-polymorph is known to be the stable phase for the end-members $Lu_2Si_2O_7$ and $Y_2Si_2O_7$. The XRD patterns of all the compositions studied are compatible with the structure of the β-polymorph. Unit cell parameters are calculated as a function of composition from XRD patterns. They show a linear change with increasing Y content, which indicates a solid solubility of β-$Y_2Si_2O_7$ in β-$Lu_2Si_2O_7$ at 1300 °C. ^{29}Si MAS NMR spectra of the different members of the system agree with the XRD results, showing a linear decrease of the ^{29}Si chemical shift with increasing Y content. Finally, a correlation reported in the literature to predict ^{29}Si chemical shifts in silicates is applied here to obtain the theoretical variation in ^{29}Si chemical shift values in the system $Lu_2Si_2O_7$–$Y_2Si_2O_7$ and the results compare favorably with the values obtained experimentally.

Keywords: Solid solution; $Y_2Si_2O_7$; $Lu_2Si_2O_7$; ^{29}Si MAS-NMR; XRD; Group electronegativity; Polymorphism; Silicates

1. Introduction

Rare earth (*RE*) pyrosilicates ($RE_2Si_2O_7$) are well known for their polymorphism. They exhibit up to eight structure types (at normal pressure) depending on the temperature and the ionic radius of the *RE* cation [1,2]. All of them contain $(Si_2O_7)^{6-}$ structural units (two silicon tetrahedra sharing one corner), except the α-polymorph which has the average pyrosilicate composition but contains $(SiO_4)^{4-}$ and $(Si_3O_{10})^{8-}$ anions in 1:1 ratio, i.e., isolated tetrahedra and chains of three Si tetrahedra.

Many structural studies have been conducted on *RE* pyrosilicates containing one type of *RE* cation. The investigation of the solid solubility between the $RE_2Si_2O_7$ structures containing different *RE* cations has been, however, very scarce [2]. The study of this subject is interesting, not only from the academic point of view, but also in the materials science field. Mixtures of refractory *RE* oxides are used as sintering aids for the fabrication of silicon nitride structural ceramics. Upon annealing, $(RE)_2Si_2O_7$ crystallizes at the grain boundaries of Si_3N_4, and improves the high temperature mechanical properties of the material [3–8]. Knowledge of the crystalline structures adopted by the $(RE)_2Si_2O_7$ intergranular phase at different temperatures and *RE* contents is therefore of great value in understanding the behavior of these materials. Several researchers have shown that the high temperature strength and oxidation resistance of Si_3N_4 are correlated with the radius of the *RE* cation in the oxide additives, such that the smaller the *RE* the better the properties of the silicon nitride [8,9]. Choi and Lee [9] showed that Y_2O_3, Lu_2O_3, and Sc_2O_3, among all lanthanide oxides, impart the highest flexural strength values to Si_3N_4. In this paper, we have selected the first two oxides to examine the phase transitions with composition in the system

*Corresponding author. Fax: +34 95 446 06 65.
E-mail address: anieto@icmse.csic.es (A.I. Becerro).

0022-4596/$ - see front matter © 2004 Elsevier Inc. All rights reserved.
doi:10.1016/j.jssc.2004.09.006

$Lu_2Si_2O_7$–$Y_2Si_2O_7$; members of this system are expected to form in the intergranular region of Si_3N_4 when mixtures of both oxides are used as sintering aids of the Si_3N_4 structural ceramic.

$Y_2Si_2O_7$ shows up to five polymorphs with increasing temperature (y, α, β, γ and δ, also called y, B, C, D and E, respectively) [2]; Ito and Johnson [10] established the following transition temperatures in $Y_2Si_2O_7$: $\alpha \overset{1225\,^\circ C}{\longrightarrow} \beta \overset{1445\,^\circ C}{\longrightarrow} \gamma \overset{1535\,^\circ C}{\leftrightarrow} \delta$. They did not include the other low temperature polymorph (y). $Lu_2Si_2O_7$ exhibits, however, a unique polymorph (β or C) up to the melting point of the compound. The study of the $Lu_{2-x}Y_xSi_2O_7$ system is therefore of special interest to analyze the stability fields of the different polymorphs with temperature and composition as well as to study the structural variations across the regions of solid solubility. In this paper, we have selected a temperature (1300 °C) at which both $Lu_2Si_2O_7$ and $Y_2Si_2O_7$ show the β polymorph as the thermodynamically stable phase, and we have studied the long- and short-range order variations of the structures appeared with increasing Y content from pure β-$Lu_2Si_2O_7$ to pure β-$Y_2Si_2O_7$.

2. Experimental section

2.1. Synthesis

The sol–gel route used for this study was derived from the synthesis of a well-homogenized gel of $Y_2Si_2O_7$ [11]. The starting materials were $Y(NO_3)_3 \cdot 6H_2O$ (99.9% Sigma), $Lu(NO_3)_3 \cdot 6H_2O$ (99.9% Sigma), $Si(OC_2H_5)_4$ (TEOS, 98% solution Sigma), HCl 35% aqueous solution and 96% ethanol. A TEOS solution in ethanol (1:3 in volume) was added over appropriate amounts of $Y(NO_3)_3 \cdot 6H_2O$, $Lu(NO_3)_3 \cdot 6H_2O$ and HCl for the preparation of $Lu_{2-x}Y_xSi_2O_7$ members with $x = 0$, 0.2, 0.5, 1.0, 1.5, 1.8 and 2.0. The mixtures were stirred at 40 °C for 72 h and the transparent gels obtained were dried at 60 °C for 24 h in air. Nitrate was eliminated by calcination at 500 °C for 1 h at a heating rate of 1 °C min^{-1}. The powder obtained in each case was subsequently calcined at a heating rate of 5 °C min^{-1} upto 1300 °C for 24 h and slowly cooled down to room temperature.

2.2. Characterization

The global composition of the samples was examined by X-ray fluorescence (X Siemens SRS-3000); Table 1 shows the agreement between the nominal and real compositions. Several complementary techniques were selected which allowed a detailed ex situ characterization of the samples. X-ray diffraction (XRD) studies were carried out using a Siemens D-501 diffractometer, with Ni-filtered Cu$K\alpha$ radiation, steps of 0.02° and counting time of 10 s. The XRD patterns were analyzed using both the Le Bail and the Rietveld methods with the GSAS software (Larson and Von Dreele) [12]. The background was previously subtracted automatically using the diffractometer software although the background intensities were subsequently refined. Lattice and profile parameters (linewidths and asymmetry parameters) were calculated by means of a Le Bail refinement. A structural refinement was then applied following the Rietveld method; the refined parameters were: background coefficients, phase fractions, lattice constants, site occupation fractions for the *RE* site and isotropic temperature factors. Powder elemental silicon was used as internal standard. ^{29}Si Magic Angle Spinning Nuclear Magnetic Resonance (MAS-NMR) spectroscopy measurements were carried out in a Bruker DRX400 (9.39 T) spectrometer equipped with a multinuclear probe, using 4 mm zirconia rotors spinning at 11 kHz. A single pulse sequence was used, with a pulse length of 2.5 μs ($\pi/2$ pulse length = 7.5 μs), an observation frequency for ^{29}Si of 79.49 MHz, and an optimized delay time of 600 s. The chemical shifts are reported in ppm from tetramethylsilane (TMS). The spectra were simulated using a modified version of the Bruker Winfit program to handle the finite spinning speed in MAS experiments [13].

Table 1
FRX analyses, ^{29}Si chemical shifts, full-width at half-maximum and fraction of Gaussian line in the Gaussian-lorentzian function (from the simulation of the experimental MAS-NMR spectra in Fig. 4), group electronegativity sums for the members of the solid solution, predicted ^{29}Si NMR chemical shifts (following Janes and Oldfield correlation [19]) and difference between the calculated and observed values

FRX		δ (obs) (ppm)	FWHM (Hz)	x [$xG/(1-x)L$]	ΣEN	δ (cal) (ppm)	Error (ppm)
x [$Lu_{2-x}Y_xSi_2O_7$] (nominal)	x [$Lu_{2-x}Y_xSi_2O_7$] (real)						
0.00	0.00	−91.70	117.6	0.05	15.25	−91.85	−0.15
0.20	0.23(1)	−91.87	130.4	0.09	15.26	−92.00	−0.13
0.50	0.56(1)	−92.05	152.6	0.32	15.27	−92.22	−0.17
1.00	0.97(1)	−92.62	158.6	0.42	15.28	−92.58	0.04
1.50	1.51(1)	−93.03	147.1	0.43	15.29	−92.95	0.08
1.80	1.79(1)	−93.38	118.6	0.25	15.30	−93.16	0.22
2.00	2.00	−93.65	47.31	0.34	15.31	−93.31	0.34

3. Results and discussion

Fig. 1 exhibits representative portions (15–50° 2θ) of the XRD diagrams of different $Lu_{2-x}Y_xSi_2O_7$ members ($x = 0.0$, 0.2, 0.5, 1.0, 1.5, 1.8 and 2.0) calcined at 1300 °C for 24 h. The diagram of the $x = 0.0$ sample matches the standard pattern of β-$Lu_2Si_2O_7$ (JCPDS chart 35-326), as expected. Increasing Y content produces very similar patterns, with variations in peak positions and intensity; see, for example, the shift of the peaks under the dashed lines, the intensity decrease of the diffraction at ca. 20° 2θ and the progressive separation of the double reflection at ca. 42.5° 2θ, marked with arrows in the figure. These variations result from changes in unit cell dimensions and composition. The diagram of the $x = 2.0$ $Lu_{2-x}Y_xSi_2O_7$ sample matches the standard pattern of β-$Y_2Si_2O_7$ (JCPDS chart 38-0440). The structure of the β-polymorph is, therefore, maintained across the $Lu_2Si_2O_7$–$Y_2Si_2O_7$ system at 1300 °C. Traces of X2-RE_2SiO_5 appear as a secondary product of the synthesis (corresponding reflections marked with asterisks). Fig. 2a shows the FWHM of several reflections for all the compositions. The crystallinity of the samples varies with the amount of yttrium, increasing from $x = 0.0$ to 0.5 (FWHM drops about 14%) and staying roughly constant up to the yttrium-rich end.

In order to calculate the dimensions of the unit cell of each member of the system, the patterns, excluding the reflections of X2-RE_2SiO_5, have been analyzed using the Le Bail and the Rietveld methods, as described in the experimental section. The starting parameters for the refinement of the structures with $x \leqslant 1$ have been taken from those reported for pure β-$Lu_2Si_2O_7$ [14] while the refinement of compositions with $x > 1$ was carried out from the parameters reported for pure β-$Y_2Si_2O_7$ [15]. Fig. 2b exhibits the observed pattern, the GSAS fitted curve and the difference curve obtained from the structural refinement of the $x = 0.5$ sample (the rest of compositions show very similar fits to this one). It can be observed that all the reflections could be fitted on the basis of a monoclinic unit cell with space group $C2/m$, as corresponds to the crystal structure of the β-polymorph. The lattice parameters as a function of Y content are shown in Fig. 3. The same size of the y-axis has been used in the three plots to appreciate relative changes in the a, b and c unit cell parameters. Both a and b lattice parameters increase linearly, at approximately the same rate, with increasing Y content, while the c parameter does not change appreciably with composition. A possible explanation for the constant value of the c unit cell parameter versus the increase of a and b can be understood from the crystal structure of β-$Lu_2Si_2O_7$ [14] represented in Fig. 3. It can be observed that the RE atoms (Lu in this case) are aligned along the c-axis, with a Lu–Lu distance of 4.71 Å. The O

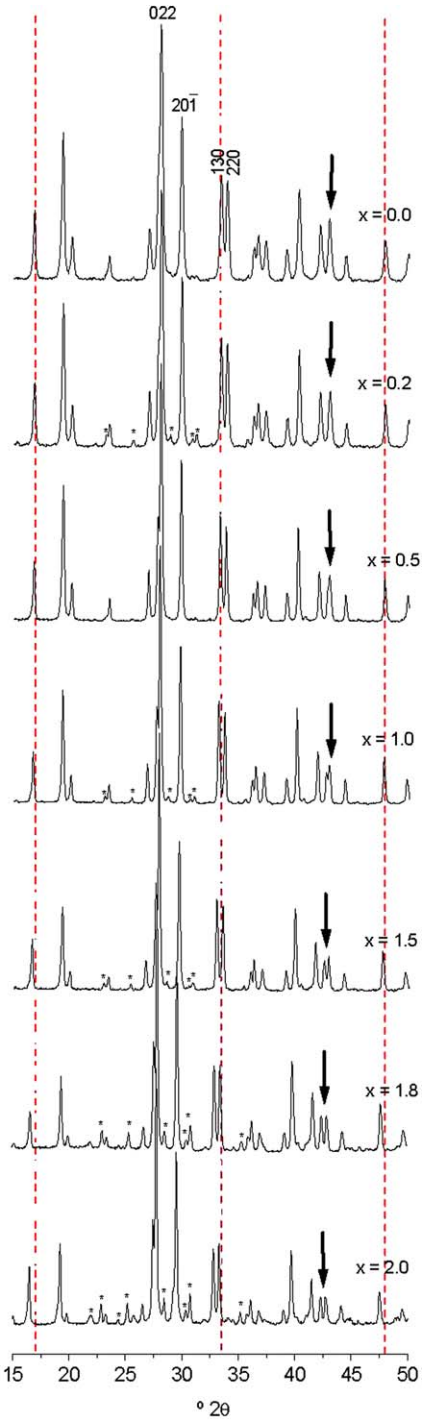

Fig. 1. Representative portions of the XRD diagrams of samples in the $Lu_{2-x}Y_xSi_2O_7$ system with $x = 0.00$, 0.20, 0.50, 1.00, 1.50, 1.80 and 2.00, calcined at 1300 °C for 24 h. Three lines have been drawn on top of three diffraction lines of the $Lu_2Si_2O_7$ XRD diagram in order to appreciate their shift to lower angles with increasing Y content. The arrow shows a double peak with separation increasing with increasing Y content. * = traces of X2-RE_2SiO_5.

neighbors of the Lu atoms are, however, distributed along both, the a and b directions, with much shorter distances (2.20 and 2.27 Å—irregular coordination

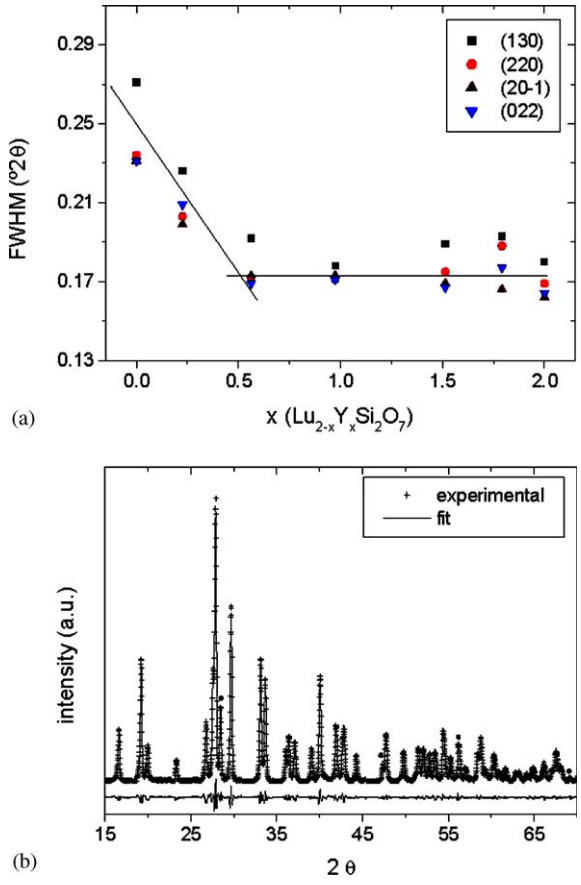

Fig. 2. (a) FWHM of reflections indexed in Fig. 1. (b) Experimental (crosses) and calculated (solid line) XRD patterns of the $x = 0.5$ $Lu_{2-x}Y_xSi_2O_7$ sample. The difference plot is also shown. Circles show the diffractions from the silicon standard.

octahedra). It seems reasonable that, on replacing Lu by a bigger atom like Y, the c unit cell dimension does not experience any size modification because there is enough room along the c-axis for the Y atoms to accommodate. However, the size of the a and b parameters increase because the bigger Y atom expands the Y–O octahedron in the a and b directions of the unit cell.

Finally, the β angle of the unit cell (Fig. 3) decreases linearly with increasing Y content while the unit cell volume increases. A linear increase in the unit cell volume with increasing the RE^{3+} ionic radius has also been reported for pure β-$RE_2Si_2O_7$ members (RE = Lu, Yb, Tm, Er and Ho) [16]. In conclusion, the linear behavior of the unit cell parameters with composition is a clear indication of the solid solubility between β-$Lu_2Si_2O_7$ and β-$Y_2Si_2O_7$ at 1300 °C.

The local environment of the Si nuclei in the members of the β-$Lu_2Si_2O_7$–β-$Y_2Si_2O_7$ system has been studied by means of ^{29}Si MAS-NMR spectroscopy (the crosses in Fig. 4 show the experimental ^{29}Si MAS-NMR spectra). All the spectra show a main ^{29}Si resonance in the ppm range characteristic of the Q^1 environments of the $[Si_2O_7]^{6-}$ units in the pyrosilicate structure. Some spectra exhibit a small contribution at ca. −78 ppm (not shown), from the secondary product X2-RE_2SiO_5. It can be easily observed from Fig. 4 that the maxima of the curves shift to lower frequency with increasing Y content. In order to obtain the chemical shift and the FWHM of each resonance, the spectra were simulated successfully (solid curve in Fig. 4) on the basis of a unique Gaussian–Lorentzian line ($= xG/(1–x)L$, where G is the Gaussian function and L the Lorentzian function). Resulting parameters are given in Table 1.

The ^{29}Si chemical shifts do vary with composition in a linear manner, as seen in Fig. 5a. The ^{29}Si chemical shifts of the end members are in agreement with the values reported in the literature for β-$Lu_2Si_2O_7$ [17] and β-$Y_2Si_2O_7$ [18]. The linear behavior of the chemical shifts with composition also support the XRD data in favor of the solid solubility between β-$Lu_2Si_2O_7$ and β-$Y_2Si_2O_7$ at 1300 °C.

Janes and Oldfield [19] proposed a ^{29}Si chemical shift correlation based on group electronegativity. The following section of this work is devoted to check that correlation in our β-$Lu_2Si_2O_7$–β-$Y_2Si_2O_7$ system. Janes and Oldfield first defined three types of silicon depending on the presence of only σ-(type S silicon), σ- and π-(type P silicon) bonded ligands or silicon coordinated to both S and P ligand types (type M silicon). For type P silicon sites, as is the case for our pyrosilicate $Lu_{2-x}Y_xSi_2O_7$ structures, they give the following correlation:

$$\delta_{Si} = -24.336\ \Sigma EN + 279.27, \quad (1)$$

where ΣEN is the group electronegativity sum. In order to use the method, the first step is to establish the group electronegativities for the various oxy-metal fragments to which Si is bonded in the pyrosilicate structure.

The group electronegativity sum of a given Q^n silicon site is determined, following Janes and Oldfield [19], as follows:

$$\Sigma EN(Q^n) = \Sigma EN_f + (4 - n)\ \Sigma(EN_{nf} z_{nf}/\Sigma z_{nf}), \quad (2)$$

where n is the number of total framework tetrahedra coordinated to a given silicon tetrahedron; in our case, $n = 1$ because we are dealing with pyrosilicate structures. EN_f and EN_{nf} represent the group electronegativity values for framework and nonframework ligands, respectively, and z_{nf} is the formal charge of a nonframework cation. In order to account for variations in the bridging-oxygen bond angles, which are believed to influence the oxygen orbital electronegativities, Janes and Oldfield [19] derived the OSi group electronegativity as a function of bridging bond angle (SiOSi) using three silica polymorphs (low quartz, low cristobalite and coesite). Albeit for only three minerals, a linear correlation of 0.99997 is observed between the group

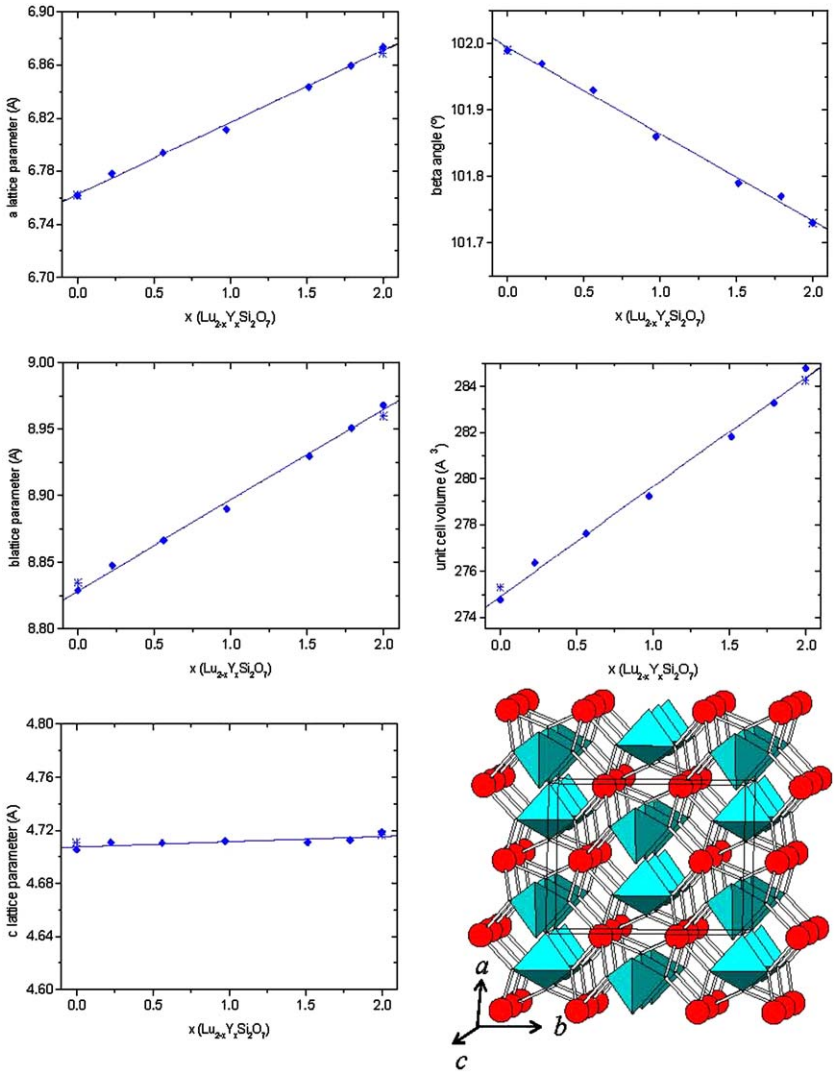

Fig. 3. Unit cell parameters (a, b, c, β and volume) plotted as a function of Y content in the system $Lu_2Si_2O_7$–$Y_2Si_2O_7$. The error bars are approximately the size of the symbols. The stars are the values found in the literature for the end-members β-$Lu_2Si_2O_7$ [14] and β-$Y_2Si_2O_7$ [15]. Down-right: Crystal structure of β-$Lu_2Si_2O_7$ based on the description by Soetebier and Urland [14]. Polyhedra correspond to SiO_4 tetrahedra while the spheres represent Lu atoms.

electronegativity and bridging bond angle as follows:

$$\mathrm{EN(OSi)} = (\angle\mathrm{SiOSi}/136.79) + 2.9235. \quad (3)$$

We have used this correlation to obtain the OSi group electronegativity in the members of our solid solution. The SiOSi bond angle is 180° for all the structures across the β-$Lu_2Si_2O_7$–β-$Y_2Si_2O_7$ join, and therefore, EN(OSi) has a constant value of 4.24 and that will be the value of $\Sigma\mathrm{EN_f}$ in Eq. (2).

Janes and Oldfield [19] obtained group electronegativities of several oxy-metal ligands but they did not show values for OLu or OY. We have calculated them empirically for the series of model compounds listed in Table 2, which include three compounds with OY groups and two with OLu groups attached to Si. We have done the calculations using Eqs. (1) and (3) (the latter when necessary) as well as the ^{29}Si chemical shifts reported in the literature for those compounds. The average values obtained in this way for OY (3.69) and OLu (3.67) have then been used for the calculation of the electronegativity sums of the Si site in our $Lu_{2-x}Y_xSi_2O_7$ system:

$$\begin{aligned}\Sigma\mathrm{EN}(\mathrm{Q}^1) &= \mathrm{EN(OSi)} + 3\Sigma(\mathrm{EN_{nf}}z_{\mathrm{nf}}/\Sigma z_{\mathrm{nf}}) = 4.24 \\ &\quad + 3\{[x\,\mathrm{EN(OY)}\,3/6] + [(2-x)\mathrm{EN(OLu)}3/6]\} \\ &= 15.25 + 0.03x. \end{aligned} \quad (4)$$

The resultant group electronegativity sums are given in Table 1, and they provide the basis for the prediction of the chemical shifts for the different members of the solid solution, which is obtained by substituting expression (4) in Eq. (1):

$$\delta_{\mathrm{Si}} = -24.336\,\Sigma\mathrm{EN} + 279.27 = -91.85 - 0.73x. \quad (5)$$

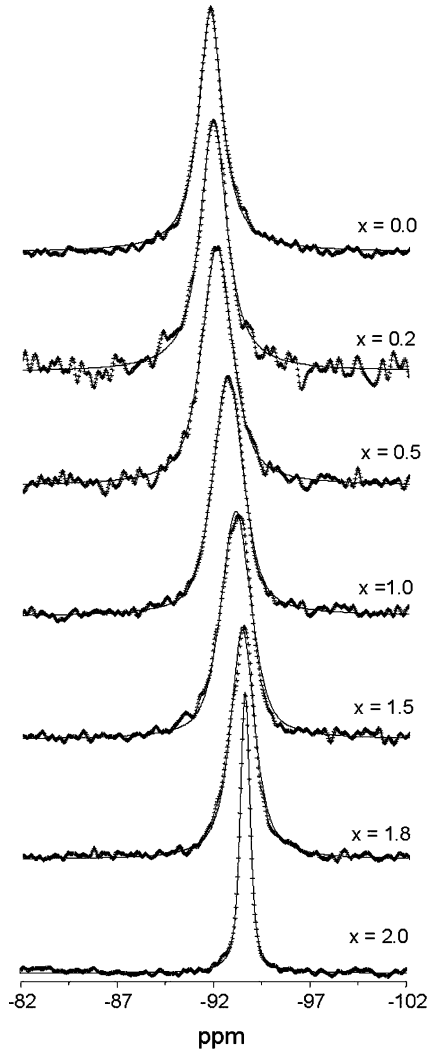

Fig. 4. Experimental (crosses) and simulated (solid line) ^{29}Si MAS-NMR spectra of samples in the $Lu_{2-x}Y_xSi_2O_7$ system.

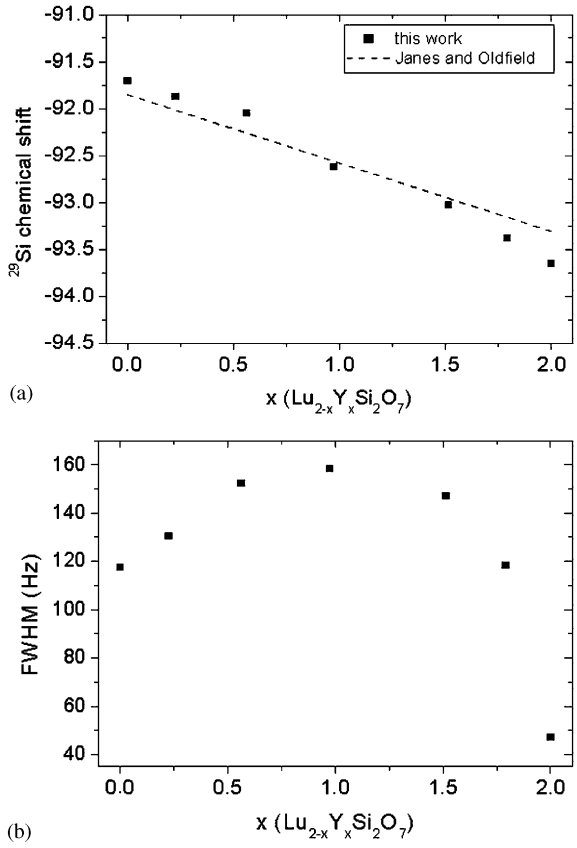

Fig. 5. (a) Squares: Experimental ^{29}Si chemical shift values plotted as a function of Y content in the system $Lu_2Si_2O_7$–$Y_2Si_2O_7$. Dashed line: ^{29}Si chemical shift values predicted from the correlation of Janes and Oldfield [19] using electronegativity group values. (b) FWHM values of the ^{29}Si MAS-NMR spectra as a function of Y content in the system $Lu_2Si_2O_7$–$Y_2Si_2O_7$.

The ^{29}Si chemical shifts obtained from Eq. (5) are shown in Table 1 and plotted versus x in Fig. 5a. It can be observed that the predicted values compare very favorably with our experimental values for ^{29}Si. The maximum difference between the calculated and the experimental chemical shift values is 0.34 ppm, which is of the order of the lowest differences presented in the work of Janes and Oldfield [19]. Although Janes and Oldfield present data for 99 Si sites in 51 different compounds, only 5 sites are of Q^1 type, the majority (67) being Q^4 sites. The present work reconfirms the goodness of their correlation, which provides chemical shift values for pyrosilicates with a minimum error.

Finally, the FWHM values obtained fitting the spectra to a unique Gaussian–Lorentzian curve and given in Table 1, have been plotted versus composition in Fig. 5b. If the degree of crystallinity of the samples were the only factors affecting the FWHM of the ^{29}Si MAS NMR peaks, then they would exhibit a similar behavior to that of the diffraction peaks (Fig. 2a). This is not the case, although it could explain the differences in FWHM values between both end-members. We think that the distribution of Y and Lu in the crystal structure of the β-$RE_2Si_2O_7$ pyrosilicate plays an important role in the FWHM values of the NMR peaks. Each silicon nucleus in the β-$RE_2Si_2O_7$ structure is surrounded by six RE atoms. A homogeneous distribution of Y and Lu atoms in the crystal structure would cause a unique type of Si environment, Si(6Lu) and Si (6Y), in both $Lu_2Si_2O_7$ and $Y_2Si_2O_7$ end-members, respectively, as well as in the $x = 1$ $Lu_{2-x}Y_xSi_2O_7$ composition –Si(3Lu, 3Y)–. On the contrary, a random distribution of Y and Lu in the crystal structure would give rise to seven different types of Si environments in any composition, namely, Si [(6−x)Lu, xY], with $x = 0$ to 6, the proportions of each depending on the Lu/Y ratio. This variety of environments would give rise to a maximum FWHM value in the spectrum of the $x = 1$ $Lu_{2-x}Y_xSi_2O_7$ composition while the FWHM value would decrease when crossing to both end members. The latter seems, therefore, to be the case of our system;

Table 2
^{29}Si chemical shifts, mean SiOSi angles and group electronegativities for a series of rare earth silicates

Group	Compound	^{29}Si chemical shift (ppm)	Mean SiOSi angle (deg)	Group electronegativity	Average group electronegativity
OY	β-$Y_2Si_2O_7$	−93.7	180	3.69	3.69
OY	γ-$Y_2Si_2O_7$	−92.7	172	3.70	
OY	X2-Y_2SiO_5	−79.4	—	3.68	
OLu	β-$Lu_2Si_2O_7$	−91.7	180	3.67	3.67
OLu	X2-Lu_2SiO_5	−77.1	—	3.66	

we have tried to fit each spectrum to the sum of those seven different Si environments but the quality of the spectra, together with the small range of ^{29}Si chemical shifts expected for the seven environments (from −91.7 to −93.7 ppm) did not allow to reach any reliable results.

4. Conclusions

A solid solution between $Lu_2Si_2O_7$ and $Y_2Si_2O_7$ is formed at 1300 °C. Yttrium is able to replace Lutetium in the *RE* crystallographic site while maintaining the structure of the β-polymorph.

The *a* and *b* unit cell parameters increase linearly with increasing Y content from $Lu_2Si_2O_7$ to $Y_2Si_2O_7$, while the *c* unit cell parameter does not change with composition. Increasing Y content produces, as well, a linear increase in the unit cell volume and a linear decrease in the β monoclinic angle. The linearity observed for the crystallographic parameters indicates solid solubility in the system β-$Lu_2Si_2O_7$–β-$Y_2Si_2O_7$.

The ^{29}Si chemical shift values increase linearly with increasing Y content. The experimental values coincide, within a minimum deviation, with those predicted from electronegativity group values with the correlation proposed by Janes and Oldfield [19]. The analysis of the FWHM of the spectra indicates that Y and Lu atoms are randomly, rather than homogenously, distributed in the crystal structure of the pyrosilicate.

Acknowledgments

We gratefully acknowledge J.M. Trillo and M.D. Alba for helpful NMR discussions and the financial support from DGICYT Projects No. BQU2001-3138 and MAT2002-03504 and Ramón y Cajal No. 2002/969.

References

[1] J. Ito, H. Johnson, Am. Mineral. 53 (1968) 1940.
[2] J. Feslche, Struct. Bonding 13 (1973) 99.
[3] A. Tsuge, K. Nishida, M. Komatse, J. Am. Ceram. Soc. 58 (1975) 323.
[4] C.H. Drummond, W.E. Lee, W.A. Sanders, J.D. Kiser, Ceram. Eng. Sci. Proc. 9 (1988) 1343.
[5] T.R. Dinger, R.S. Rai, G. Thomas, J. Am. Ceram. Soc. 71 (1988) 236.
[6] I.H. Arita, D.S. Wilkinson, G.R. Purdy, J. Am. Ceram. Soc. 75 (1992) 3315.
[7] P. Vomacka, O. Babushkin, J. Eur. Ceram. Soc. 15 (1995) 921.
[8] Z.L. Hong, H. Yoshida, Y. Ikuhara, T. Sakuma, T. Nishimura, M. Mitomo, J. Eur. Ceram. Soc. 22 (2002) 527.
[9] H.J. Choi, J.G. Lee, Y.W. Kim, J. Mater. Sci. 32 (1997) 1937.
[10] J. Ito, H. Johnson, Am. Mineral. 53 (1968) 1940.
[11] M. Díaz, I. García-Cano, S. Mello-Castanho, J.S. Moya, M.A. Rodríguez, J. Non-Crystal. Solids 289 (2001) 151.
[12] A.C. Larson, R.B. Von Dreele, GSAS: General Structural Analysis system, Los Alamos National Laboratory, Los Alamos, NM. The Regents of the University of California, 1994.
[13] D. Massiot, F. Fayon, M. Capron, I. King, S. Le Calvé, B. Alonso, J.O. Durand, B. Bujoli, Z. Gan, G. Hoatson, Magn. Reson. Chem. 40 (2002) 70.
[14] F. Soetebier, W. Urland, Z. Kristallogr. NCS 217 (2002) 22.
[15] G.J. Redhammer, G. Roth, Acta Crystallogr. C 59 (2003) 1103.
[16] J. Feslche, Less Common Metals 21 (1970) 1.
[17] A.I. Becerro, Ph.D. Thesis, University of Seville, 1997.
[18] J. Parmentier, P.R. Bodart, L. Audoin, G. Massouras, D.P. Thompson, R.K. Harris, P. Goursat, J.L. Bessons, J. Solid State Chem. 149 (2000) 16.
[19] N. Janes, E. Oldfield, J. Am. Chem. Soc. 107 (1985) 6769.